

Electroweak two-loop corrections to $\sin^2 \theta_{\text{eff}}^{b\bar{b}}$ and R_b using numerical Mellin-Barnes integrals

AYRES FREITAS, YI-CHENG HUANG

*Pittsburgh Particle-physics Astro-physics & Cosmology Center (PITT-PACC),
Department of Physics & Astronomy, University of Pittsburgh, Pittsburgh, PA 15260, USA*

Abstract

Multi-loop integrals can be evaluated numerically using Mellin-Barnes representations. Here this technique is applied to the calculation of electroweak two-loop correction with closed fermion loops for two observables: the effective weak mixing angle for bottom quarks, $\sin^2 \theta_{\text{eff}}^{b\bar{b}}$, and the branching ratio of the Z boson into bottom quarks, R_b . Good agreement with a previous result for $\sin^2 \theta_{\text{eff}}^{b\bar{b}}$ is found. The result for R_b is new and it turns out that the electroweak two-loop corrections are relatively large – of the same order as the current experimental uncertainty. A simple parametrization formula is provided which approximates the full result within integration errors.

1 Introduction

High-precision data from LEP, SLC, the Tevatron, and the LHC allow us to perform very accurate tests of the Standard Model (SM), predict the mass of the Higgs boson, and possibly identify hints for new physics. For this purpose, the experimental results are compared to theoretical computations including higher-order radiative corrections. For some of the most precisely determined observables it is necessary to include complete two-loop corrections in the calculation. Such calculations have been carried out for the mass of the W boson, M_W [1–3], and the effective weak mixing angle $\sin^2 \theta_{\text{eff}}$ parametrizing the ratio of vector and axial-vector couplings of the Z boson to leptons [4–6], light quarks [5], and bottom quarks [7]. Furthermore, partial electroweak three-loop contributions [8], as well as three-loop [10, 11] and leading four-loop [12] QCD corrections to these observables have been determined. The two-loop and leading three-loop results for M_W and $\sin^2 \theta_{\text{eff}}$ have been implemented in commonly used SM fit programs such as ZFITTER [13] and GFITTER [14].

A major difficulty in these calculations are two-loop integrals with multiple mass and momentum scales. In general these integrals cannot be solved analytically in closed form, so that one has to use numerical methods instead. Numerical techniques for the evaluation of loop integrals face two main challenges: extraction of ultraviolet (UV) and infrared (IR) singularities, as well as stability and efficiency of the numerical integrations. A powerful method is based on Mellin-Barnes (MB) representations. It has been demonstrated that MB representations can be used to isolate the singularities of an arbitrary multi-loop integral in a systematic way [15, 16], such that this procedure can be automated in a computer program [16, 17]. Furthermore, it was shown that the integration time and convergence behavior of the MB integrals can be improved substantially by suitable variable transformations and by analytically integrating over some variables of the multi-dimensional MB integrals [18].

This article reports on the concrete calculation of two electroweak precision observables using the technique described in Ref. [18]. First, the method is validated by reproducing the result for the fermionic electroweak two-loop corrections to the effective weak mixing angle of bottom quarks, $\sin^2 \theta_{\text{eff}}^{bb}$, published earlier in Ref. [7]. Here the term “fermionic” refers to diagrams with at least one closed fermion loop. Secondly, a new result is presented for the complete fermionic electroweak two-loop (next-to-next-leading order) corrections to R_b , the branching ratio of the Z boson into bottom quarks and all quarks. Until now, only an approximate results for the electroweak two-loop corrections to the Z partial widths are available, using an expansion for large values of the top-quark mass. For decays of the Z boson into quarks of the first two generations, this expansion has been driven to the order $\mathcal{O}(\alpha^2 m_t^2)$ [19], while for the $Z \rightarrow b\bar{b}$ width only the leading $\mathcal{O}(\alpha^2 m_t^4)$ coefficient is known [20].

As elaborated in the next section, the radiative corrections for both $\sin^2 \theta_{\text{eff}}^{bb}$ and R_b are obtained from the same loop diagrams of the $Z f \bar{f}$ vertex. For the calculation presented here, the MB method of Ref. [18] has been used for the most difficult two-loop diagrams involving triangle sub-loops. The remaining diagrams have been computed by reducing the relevant integrals to a set of master integrals [21], which are then evaluated numerically [5, 22]. These steps are described in more detail in section 3. Finally, numerical results for both observables are presented in section 4, and the main findings are summarized in section 5.

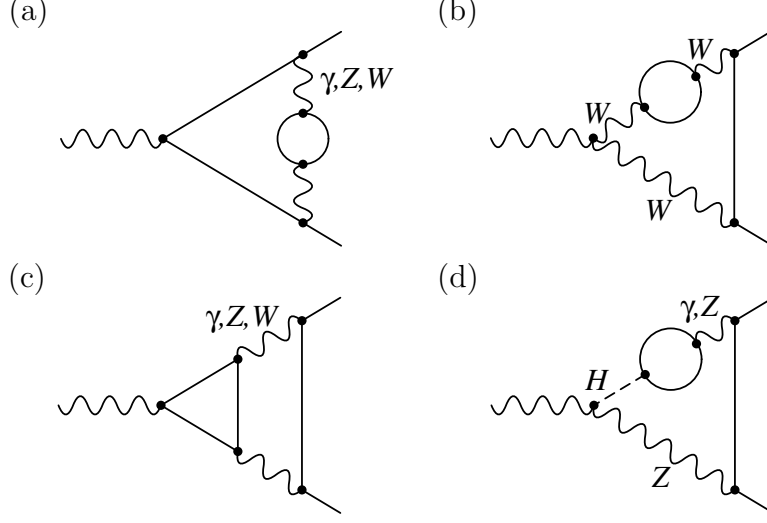


Figure 1: Fermionic electroweak two-loop $Zf\bar{f}$ vertex diagrams contributing to the vertex form factors $v_f^{(2)}$ and $a_f^{(2)}$.

2 $\sin^2 \theta_{\text{eff}}^{b\bar{b}}$ and R_b at next-to-next-to-leading order

The effective weak mixing angle $\sin^2 \theta_{\text{eff}}^{f\bar{f}}$ is related to the ratio of vector and axial-vector couplings, v_f and a_f of the $Zf\bar{f}$ vertex, *i. e.*

$$\sin^2 \theta_{\text{eff}}^{f\bar{f}} \equiv \frac{1}{4} \left(1 + \Re e \frac{v_f}{a_f} \right). \quad (1)$$

Expanding this definition to next-to-next-to-leading order (NNLO) one obtains

$$\sin^2 \theta_{\text{eff}}^{f\bar{f}} = \left(1 - \frac{\overline{M}_W^2}{\overline{M}_Z^2} \right) \Re e \left\{ 1 + \frac{a_f^{(1)} v_f^{(0)} - v_f^{(1)} a_f^{(0)}}{a_f^{(0)} (a_f^{(0)} - v_f^{(0)})} \Big|_{k^2=M_Z^2} + \frac{a_f^{(2)} v_f^{(0)} a_f^{(0)} - v_f^{(2)} (a_f^{(0)})^2 - (a_f^{(1)})^2 v_f^{(0)} + a_f^{(1)} v_f^{(1)} a_f^{(0)}}{(a_f^{(0)})^2 (a_f^{(0)} - v_f^{(0)})} \Big|_{k^2=M_Z^2} \right\}, \quad (2)$$

where $v_f^{(0,1,2)}$ denote the tree-level, one-loop, and two-loop contributions to the vector form factor, respectively, and $a_f^{(0,1,2)}$ are defined similarly for the axial-vector form factor. Figure 1 shows the types of two-loop diagrams with closed fermions loops that contribute to $v_f^{(2)}$ and $a_f^{(2)}$. \overline{M}_W^2 and \overline{M}_Z^2 are the real parts of the gauge-invariant propagator poles of the W and Z boson, respectively. In eq. (2) the infrared (IR) divergent QED and QCD contributions cancel exactly, see for example Ref. [5], so that it is sufficient to only include IR-finite weak loop corrections.

The branching ratio R_b is defined as the ratio of the partial decay widths of the Z -boson decay into bottom quarks and into all quarks:

$$R_b \equiv \frac{\Gamma_b}{\Gamma_{\text{had}}} = \frac{\Gamma_b}{\Gamma_d + \Gamma_u + \Gamma_s + \Gamma_c + \Gamma_b} = \frac{1}{1 + 2(\Gamma_d + \Gamma_u)/\Gamma_b}, \quad (3)$$

where Γ_f stands for the partial decay width into the $f\bar{f}$ final state. In the last step in (3), the relationships $\Gamma_u \approx \Gamma_c$ and $\Gamma_d \approx \Gamma_s$ have been used, which hold to very good approximation.

Up to next-to-next-to-leading order ($q = u, d$),

$$\begin{aligned} \frac{\Gamma_q}{\Gamma_b} = & \frac{G_q^{(0)}}{G_b^{(0)}} + \frac{2}{(G_b^{(0)})^2} \Re \left\{ G_b^{(0)} G_q^{(1)} - G_q^{(0)} G_b^{(1)} \right\} + \frac{1}{(G_b^{(0)})^2} [G_b^{(0)} \mathcal{R}_q^{(1)} - G_q^{(0)} \mathcal{R}_b^{(1)}] \\ & + \frac{1}{(G_b^{(0)})^3} \Re \left\{ (G_b^{(0)})^2 [2G_q^{(2)} + (a_q^{(1)})^2 + (v_q^{(1)})^2] \right. \\ & \quad - G_b^{(0)} G_q^{(0)} [2G_b^{(2)} + (a_b^{(1)})^2 + (v_b^{(1)})^2] \\ & \quad \left. - 4G_b^{(0)} G_q^{(1)} G_b^{(1)} + 4G_q^{(0)} (G_b^{(1)})^2 \right\} \\ & + \frac{1}{(G_b^{(0)})^2} [G_b^{(0)} \mathcal{R}_q^{(2)} - G_q^{(0)} \mathcal{R}_b^{(2)} - G_b^{(0)} \mathcal{R}_q^{(1)} \mathcal{R}_b^{(1)} + G_q^{(0)} (\mathcal{R}_b^{(1)})^2] \\ & + \frac{2}{(G_b^{(0)})^3} [(G_b^{(0)})^2 (a_q^{(0)} a_q^{(1)} \mathcal{R}_{q,A}^{(1)} + v_q^{(0)} v_q^{(1)} \mathcal{R}_{q,V}^{(1)}) - G_b^{(0)} G_b^{(1)} \mathcal{R}_q^{(1)} \\ & \quad + G_q^{(0)} G_b^{(1)} \mathcal{R}_b^{(1)} + G_q^{(0)} a_b^{(0)} v_b^{(0)} (a_b^{(0)} v_b^{(1)} + v_b^{(0)} a_b^{(1)}) (\mathcal{R}_{b,A}^{(1)} - \mathcal{R}_{b,V}^{(1)}) \\ & \quad - G_b^{(0)} G_q^{(1)} \mathcal{R}_b^{(1)}], \end{aligned} \quad (4)$$

with

$$G_q^{(n)} = a_q^{(0)} a_q^{(n)} + v_q^{(0)} v_q^{(n)}, \quad \mathcal{R}_q^{(n)} = (a_q^{(0)})^2 \mathcal{R}_{q,A}^{(n)} + (v_q^{(0)})^2 \mathcal{R}_{q,V}^{(n)}. \quad (5)$$

Here $\mathcal{R}_{q,V}^{(n)}$ and $\mathcal{R}_{q,A}^{(n)}$ incorporate the n -loop QED and QCD corrections to the vector and axial-vector form factors, which have been calculated already several years ago [23, 24], see also Ref. [25]. The relevant parts for this calculation are given by

$$\mathcal{R}_{d,V}^{(1)} = \mathcal{R}_{d,A}^{(1)} = \mathcal{R}_{b,V}^{(1)} = \frac{\alpha}{12\pi} + \frac{\alpha_s}{\pi}, \quad (6)$$

$$\mathcal{R}_{u,V}^{(1)} = \mathcal{R}_{u,A}^{(1)} = \frac{\alpha}{3\pi} + \frac{\alpha_s}{\pi}, \quad (7)$$

$$\mathcal{R}_{b,A}^{(1)} = \mathcal{R}_{b,V}^{(1)} - 6 \frac{m_b^2}{M_Z^2}, \quad (8)$$

$$\mathcal{R}_{d,V}^{(2)} = -\frac{\alpha\alpha_s}{36\pi^2} + C_2 \left(\frac{\alpha_s}{\pi} \right)^2 + C_3 \left(\frac{\alpha_s}{\pi} \right)^3, \quad (9)$$

$$\mathcal{R}_{d,A}^{(2)} = \mathcal{R}_{d,V}^{(2)} - I_2 \left(\frac{M_Z^2}{m_t^2} \right) \left(\frac{\alpha_s}{\pi} \right)^2 - I_3 \left(\frac{M_Z^2}{m_t^2} \right) \left(\frac{\alpha_s}{\pi} \right)^3, \quad (10)$$

$$\mathcal{R}_{u,V}^{(2)} = \mathcal{R}_{d,V}^{(2)} - \frac{\alpha\alpha_s}{12\pi^2}, \quad (11)$$

$$\mathcal{R}_{u,A}^{(2)} = \mathcal{R}_{d,A}^{(2)} - \frac{\alpha\alpha_s}{12\pi^2}, \quad (12)$$

$$\mathcal{R}_{b,V}^{(2)} = \mathcal{R}_{d,V}^{(2)} + 12 \frac{m_b^2}{M_Z^2} \frac{\alpha_s}{\pi} + \mathcal{O}(m_b^4 \alpha_s, m_b^2 \alpha_s^2), \quad (13)$$

$$\mathcal{R}_{b,A}^{(2)} = \mathcal{R}_{d,A}^{(2)} - 22 \frac{m_b^2}{M_Z^2} \frac{\alpha_s}{\pi} - 6 \frac{m_b^4}{M_Z^4} + \mathcal{O}(m_b^4 \alpha_s, m_b^2 \alpha_s^2). \quad (14)$$

Here three-loop QCD corrections are also included in the $\mathcal{R}^{(2)}$ terms, and m_b is defined in the $\overline{\text{MS}}$ -scheme. In the power-counting the small bottom quark mass is treated to be parametrically of the same order as the fine-structure constant, $\frac{m_b^2}{M_Z^2} \sim \alpha$, so that only the leading tree-level m_b -dependence is included in (8) and the leading one-loop m_b -dependence in (13), (14). Note that the dependence on C_2 and C_3 drops out in the final result for R_b . The functions I_2 and I_3 read

$$I_2(x) = -\frac{37}{12} + \log x + \frac{7}{81}x + 0.0132x^2, \quad (15)$$

$$I_3(x) = -\frac{5075}{216} + \frac{23}{6}\zeta_2 + \zeta_3 + \frac{67}{18}\log x + \frac{23}{12}\log^2 x. \quad (16)$$

The vertex form factors $v_f^{(2)}$ and $a_f^{(2)}$ include all electroweak two-loop diagrams, as shown in Fig. 1, except those that involve IR-divergent photon exchange contributions between the outgoing fermion lines (represented by Fig. 1 (a) when both wiggly lines are photons). For the effective weak mixing angle $\sin^2 \theta_{\text{eff}}$ these QED diagrams cancel in the final result, as pointed out in Ref. [5]. For the branching fraction R_b , on the other hand, the QED contributions are included in the radiator functions $\mathcal{R}_{q,V}$ and $\mathcal{R}_{q,A}$. In consequence, for both observables, the IR-divergent QED diagrams are excluded from the calculation of the electroweak two-loop corrections discussed here.

For the renormalization the on-shell scheme is employed. In particular, the renormalized squared masses are defined as the real part of the propagator poles (which is different than the pole of the real part of the propagator). Furthermore, the external fields are renormalized to unity at the position of the poles. Details and explicit expressions for the renormalization constants can be found in Ref. [2].

For the computation of the electroweak two-loop corrections, the masses and Yukawa couplings of all fermions except the top quark can be safely neglected. Moreover, the CKM matrix is approximated by the unit matrix.

3 Outline of the computation of two-loop diagrams

Let us start by giving a brief overview to the use of MB representations for the numerical evaluation of multi-loop integrals. For more details, see Refs. [15, 16, 18].

After introduction of Feynman parameters, a general one-loop integral with N propagators can be written in the form

$$I = (-1)^N \Gamma(N - D/2) \int_0^1 dx_1 \cdots dx_N \frac{\delta(1 - x_1 - \dots - x_N)}{\left[\sum_{i,j=1}^N K_{ij} x_i x_j + \sum_{i=1}^N L_i x_i + M - i\epsilon \right]^{N-D/2}}, \quad (17)$$

where D is the number of space-time dimensions, and K_{ij} , L_i , and M depend on the masses

and external momenta of the propagators. Using the MB representation,

$$\frac{1}{(A_0 + \dots + A_m)^Z} = \frac{1}{(2\pi i)^m} \int_{\mathcal{C}_1} dz_1 \dots \int_{\mathcal{C}_m} dz_m A_1^{z_1} \dots A_m^{z_m} A_0^{-Z-z_1-\dots-z_m} \times \frac{\Gamma(-z_1) \dots \Gamma(-z_m) \Gamma(Z+z_1+\dots+z_m)}{\Gamma(Z)}, \quad (18)$$

the integral I can be transformed into a form that depends on the Feynman parameters only in terms of exponentials $x_i^{z_i}$. The integration contours \mathcal{C}_i for z_i are straight lines parallel to the imaginary axis chosen such that all arguments of the gamma functions have positive real parts. MB representations for multi-loop integrals can be obtained recursively. After integration over the Feynman parameters, the remaining MB integrals only depend on gamma functions of the integration variables and on the external parameters. For example, the “sunset” two-loop diagram is given by the MB integral

$$\begin{aligned} \text{Sunset Diagram} &= \frac{-1}{(2\pi i)^3} \int dz_1 dz_2 dz_3 (m_1^2)^{-\varepsilon-z_1-z_2} (m_2^2)^{z_2} (m_3^2)^{1-\varepsilon+z_1-z_3} (-p^2)^{z_3} \\ &\quad \times \Gamma(-z_2) \Gamma(-z_3) \Gamma(1+z_1+z_2) \Gamma(z_3-z_1) \\ &\quad \times \frac{\Gamma(1-\varepsilon-z_2) \Gamma(\varepsilon+z_1+z_2) \Gamma(\varepsilon-1-z_1+z_3)}{\Gamma(2-\varepsilon+z_3)}, \end{aligned} \quad (19)$$

with $\varepsilon = (4-D)/2$. All UV and IR singularities are now in the poles of the gamma functions and can be extracted in a systematic way, see Refs. [15, 16].

The remaining integrals in z_i over the complex contours \mathcal{C}_i can, in principle, be carried out numerically. However, in practice, the integrand is often highly oscillatory and the integral, while formally existent, may converge too slowly.

In Ref. [18], two effective methods for improving the convergence behavior of the numerical z_i integrals have been discussed. One modification consists in rotating the z_i -integration contours in the complex plane, which can produce an additional exponentially damped term in the integrand, so that the integral vanishes faster for $|z_i| \rightarrow \infty$. By rotating the contours for all variables z_i in parallel it is ensured that no poles of the gamma functions cross the contour. Secondly, some integrations of the multi-dimensional MB integral can be performed analytically with the help of the convolution theorem for Mellin transforms. For typical two-loop vertex diagrams needed for the calculation of the NNLO corrections to the $Zb\bar{b}$ interaction, one can treat about half of the integrations in this way, and only the remaining half will be carried out numerically. With these improvements, it was shown in Ref. [18] that the most complicated scalar integrals needed for the NNLO $Zb\bar{b}$ corrections can be evaluated in a few hours on a single-core computer.

In this work, the MB method has been used for the most complicated integrals stemming from the diagrams with triangle sub-loops, see Fig. 1 (c). The remaining two-loop integrals have been calculated by first reducing them to a set of master integrals using integration-by-parts and Lorentz identity relations [21]. Analytical formulas are known for the one-loop and two-loop vacuum master integrals, while the two-loop selfenergy and vertex master integrals have been evaluated numerically using dispersion relations as described in Ref [5, 22].

Parameter	Experimental value
M_Z	$(91.1876 \pm 0.0021) \text{ GeV}$
Γ_W	$(2.4952 \pm 0.0023) \text{ GeV}$
M_W	$(80.399 \pm 0.023) \text{ GeV}$
Γ_W	$(2.085 \pm 0.042) \text{ GeV}$
m_t	$(173.2 \pm 0.9) \text{ GeV}$
$\Delta\alpha(M_Z)$	0.05900 ± 0.00033
$m_b^{\overline{\text{MS}}}$	4.20 GeV
$\alpha_s(M_Z)$	0.1184 ± 0.0007
G_μ	$1.16637 \times 10^{-5} \text{ GeV}^{-2}$

Table 1: *Input parameters and their experimental values, from Refs. [26, 27]. The electroweak two-loop corrections of the $Zb\bar{b}$ vertex depend only the first group of parameters.*

4 Results

The computational method described in the previous section has been applied to the calculation of two-loop corrections to $\sin^2 \theta_{\text{eff}}^{b\bar{b}}$ and R_b . Both quantities depend on the input parameters listed in the upper part of Tab. 1. Note that the experimentally quoted values for the W - and Z -boson masses correspond to a Breit-Wigner parametrization with a energy-dependent width, and they have to be translation to the pole-mass scheme used in the loop calculation [28]. In effect, this translation results in a downward shift of M_W and M_Z by $\Gamma_W^2/(2M_W)$ and $\Gamma_Z^2/(2M_Z)$, respectively, where $\Gamma_{W,Z}$ and width of the gauge bosons. $\Delta\alpha(M_Z)$ is the contribution from light fermions (all fermions except the top quark) to the running of the electromagnetic coupling between the scales $Q = 0$ and M_Z .

Let us first discuss of the effective weak mixing angle of bottom quarks, $\sin^2 \theta_{\text{eff}}^{b\bar{b}}$. The fermionic two-loop corrections to this quantity have already been calculated earlier [7], so that this result can be used as an additional check of the MB method. The comparison is shown in Tab. 2 in terms of the two-loop correction factor in the second line of eq. (2):

$$\Delta\kappa_{b\bar{b}}^{(\alpha^2, \text{ferm})} = \frac{a_b^{(2)} v_b^{(0)} a_b^{(0)} - v_b^{(2)} (a_b^{(0)})^2 - (a_b^{(1)})^2 v_b^{(0)} + a_b^{(1)} v_b^{(1)} a_b^{(0)}}{(a_b^{(0)})^2 (a_b^{(0)} - v_b^{(0)})} \bigg|_{k^2=M_Z^2} \quad (20)$$

The two calculations agree to within about 1% of the two-loop contribution, which is the same order as the uncertainty from the numerical MB integration.

Next, we turn to the presentation of results for the branching ratio R_b . Table 3 lists the effects of various radiative correction terms, starting with the one-loop contribution, corresponding to the first line of eq. (4). The third column of Tab. 3 shows the new result for the purely electroweak contributions from two-loop diagrams with closed fermion loops.

M_W [GeV]	m_t [GeV]	$\Delta\kappa_{b\bar{b}}^{(\alpha^2, \text{ferm})} \times 10^3$	
		Ref. [7]	this work
80.399	171.2	-2.278	-2.303
80.399	172.2	-2.331	-2.357
80.399	173.2	-2.386	-2.410
80.399	174.2	-2.441	-2.464
80.399	175.2	-2.496	-2.518
80.422	173.2	-2.402	-2.427
80.445	173.2	-2.418	-2.444

Table 2: Results for the two-loop correction factor $\Delta\kappa_{b\bar{b}}^{(\alpha^2, \text{ferm})}$ to $\sin^2 \theta_{\text{eff}}^{b\bar{b}}$, for different values of M_W and m_t . The other input values have been set to $M_Z = 91.1876$ GeV, $M_H = 100$ GeV, $\Delta\alpha = 0$. The values obtained in this work are compared to the results of Ref. [7].

The fourth includes the electroweak two-loop corrections together with final-state corrections of order $\mathcal{O}(\alpha_s^2, \alpha_s^3, \alpha\alpha_s)$, *cf.* the last four lines of (4). Finally, higher-order two-loop QCD corrections of order $\mathcal{O}(\alpha\alpha_s)$ [29] to internal gauge-boson selfenergies, as well as three-loop QCD corrections of order $\mathcal{O}(\alpha\alpha_s^2)$ to the ρ -parameter [10] are given in the last column of the table. Additional higher-order corrections to the ρ -parameter [8, 9, 11, 12] are very small and have not been included in the numerical analysis.

As evident from the table, the electroweak two-loop corrections are relatively large compared to the one-loop results, and they are comparable to the experimental uncertainty for R_b of 6.6×10^{-4} [26]. The two-loop contribution depends only mildly on the Higgs-boson mass, see Fig. 2. Its overall effect is a reduction of the SM prediction for R_b . It is interesting to note that the electroweak two-loop corrections, the final-state QED and QCD corrections, and the higher-order QCD contributions to internal gauge-boson lines all produce a negative shift of the predicted values for R_b . The uncertainty in the prediction for R_b due to the numerical MB integration error is about 4×10^{-6} , *i. e.* less than 1% of the electroweak two-loop contribution.

The numerical results in Tab. 3 and Fig. 2 have been obtained with a fixed value of the W -boson mass. In global SM fits, however, M_W is calculated from the Fermi constant G_μ . In Refs. [1–3] this calculation has been carried out including full two-loop and partial higher-order corrections. Using the same order of perturbation theory for the calculation of M_W and R_b , the numerical results for R_b in this scheme are given in Tab. 4 and Fig. 2. As evident from the figure, the higher-order corrections beyond the one-loop level are sizeable. The most precise result including electroweak two-loop and QCD three-loop corrections has a mild tension of about two standard deviations with the experimental value $R_b = 0.21629 \pm 0.00066$ [26].

The evaluation of the complete fermionic two-loop result with the MB integrals takes several CPU-hours for one set of parameters and thus is not suitable for direct incorporation in SM fit programs. However, the prediction for R_b can be approximated to a good precision

M_H [GeV]	$\mathcal{O}(\alpha) + \text{FSR}_{1\text{-loop}}$ [10^{-3}]	$\mathcal{O}(\alpha_{\text{ferm}}^2)$ [10^{-4}]	$\mathcal{O}(\alpha_{\text{ferm}}^2) + \text{FSR}_{>1\text{-loop}}$ [10^{-4}]	$\mathcal{O}(\alpha\alpha_s, \alpha\alpha_s^2)$ [10^{-4}]
100	-3.632	-6.569	-9.333	-0.404
200	-3.651	-6.573	-9.332	-0.404
400	-3.675	-6.581	-9.331	-0.404
600	-3.690	-6.580	-9.325	-0.404
1000	-3.711	-6.568	-9.306	-0.403

Table 3: Results for electroweak one- and two-loop corrections to R_b , as defined in eqs. (3,4), for different values of M_H . The other input values are taken from Tab. 1, with a fixed value for M_W . Also shown are the effects of two- and three-loop QCD corrections to the final state (fourth column) and to gauge-boson selfenergies (fifth column). Here “FSR” stands for the final-state radiative QCD and QED corrections described by the radiator functions $\mathcal{R}^{(n)}$.

M_H [GeV]	tree-level + $\mathcal{O}(\alpha)$ + $\text{FSR}_{1\text{-loop}}$	$\mathcal{O}(\alpha_{\text{ferm}}^2) + \text{FSR}_{>1\text{-loop}}$ + $\mathcal{O}(\alpha\alpha_s, \alpha\alpha_s^2)$ [10^{-4}]	total
100	0.21562	-8.739	0.21475
200	0.21564	-8.706	0.21477
400	0.21565	-8.671	0.21479
600	0.21566	-8.655	0.21480
1000	0.21567	-8.640	0.21481

Table 4: Results for R_b , as in Table 3, but now with M_W calculated from G_μ using the SM prediction. The other input values are taken from Tab. 1.

by a simple parametrization formula:

$$R_b = R_b^0 + c_1 L_H + c_2 L_H^2 + c_3 L_H^4 + c_4 (\Delta_H^2 - 1) + c_5 \Delta_\alpha + c_6 \Delta_t + c_7 \Delta_t L_H + c_8 \Delta_{\alpha_s} + c_9 \Delta_Z, \quad (21)$$

with

$$L_H = \ln \frac{M_H}{100 \text{ GeV}}, \quad \Delta_H = \frac{M_H}{100 \text{ GeV}}, \quad \Delta_t = \left(\frac{m_t}{173.2 \text{ GeV}} \right)^2 - 1, \\ \Delta_\alpha = \frac{\Delta\alpha}{0.05900} - 1, \quad \Delta_{\alpha_s} = \frac{\alpha_s(M_Z)}{0.1184} - 1, \quad \Delta_Z = \frac{M_Z}{91.1876 \text{ GeV}} - 1. \quad (22)$$

The numerical coefficients are determined by a fit to the full numerical result, which includes all radiative corrections mentioned above: the complete $\mathcal{O}(\alpha)$ and fermionic $\mathcal{O}(\alpha^2)$ contributions to the $Zf\bar{f}$ vertex form factors, as well as virtual $\mathcal{O}(\alpha\alpha_s)$ and $\mathcal{O}(\alpha\alpha_s^2)$ corrections and final-state radiation of order $\mathcal{O}(\alpha^n)$, ($n = 1, 2, 3$) and $\mathcal{O}(\alpha\alpha_s)$. For the W -boson mass

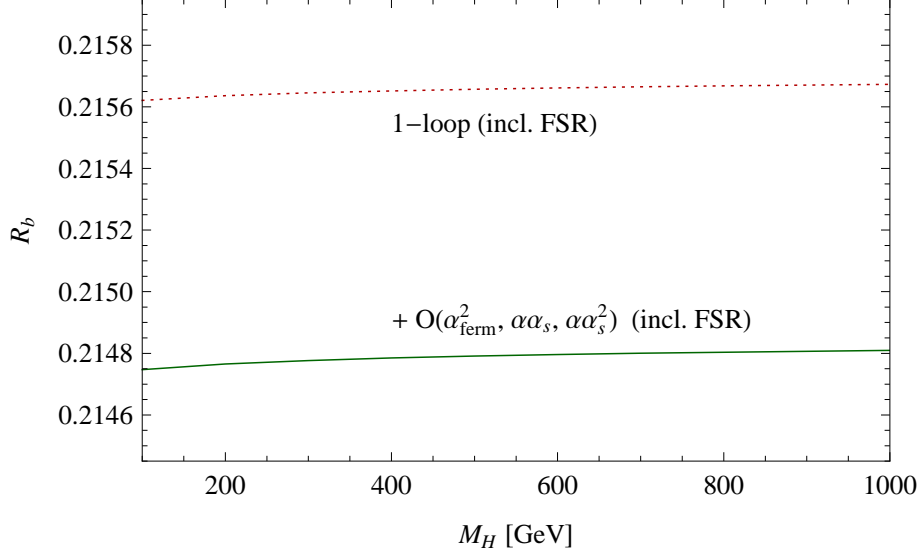


Figure 2: One-loop and two-loop (with QCD three-loop contributions) result for the branching fraction R_b as a function of M_H , and using the SM prediction for M_W to the same order of perturbation theory. Input values for the other parameters are taken from Tab. 1.

the currently most precise result of Ref. [3] is used. With these ingredients, the fit result for the coefficients is

$$\begin{aligned}
 R_b^0 = 0.2147464, \quad & c_1 = 2.21 \times 10^{-5}, \quad c_2 = 2.6 \times 10^{-6}, \quad c_3 = -6.7 \times 10^{-7}, \\
 & c_4 = 9.11 \times 10^{-8}, \quad c_5 = 6.47 \times 10^{-4}, \quad c_6 = -3.239 \times 10^{-3}, \\
 & c_7 = 6.73 \times 10^{-5}, \quad c_8 = -3.24 \times 10^{-4}, \quad c_9 = 6.10 \times 10^{-2}.
 \end{aligned} \tag{23}$$

With this parametrization the full result is approximated to better than 10^{-6} for $10 \text{ GeV} \leq M_H \leq 1 \text{ TeV}$ and the other input parameters in their 2σ experimental error ranges.

5 Summary

Mellin-Barnes representations provide a generic framework for evaluating multi-loop integrals numerically. They can be used to systematically extract all physical singularities of a given loop diagram. Furthermore, by using appropriate variable mappings and contour deformations one can achieve good numerical convergence of the Mellin-Barnes integrals for a large class of loop diagrams, see Ref. [18].

This paper reports on the application of this method to the calculation of fermionic electroweak two-loop corrections to the effective weak mixing angle for bottom quarks, $\sin^2 \theta_{\text{eff}}^{b\bar{b}}$, and the branching ratio of the Z boson into bottom quarks, R_b . These two observables have been measured to high accuracy by experiments at LEP and SLC, and they play an important role in precision tests of the Standard Model, as well as new physics models. Therefore one needs theoretical predictions for these quantities with an error that is comparable or

less than the experimental uncertainty, which requires the inclusion of electroweak two-loop corrections.

In the work presented here, the numerical Mellin-Barnes method has been used for the most difficult two-loop vertex diagrams. For the one-loop and remaining two-loop diagrams, a technique based on tensor reduction to a set of well-known master integrals has been employed, which is faster but less general than the Mellin-Barnes method.

The results for $\sin^2 \theta_{\text{eff}}^{b\bar{b}}$ have been compared to a previous calculation of the fermionic two-loop corrections with a different method Ref. [7]. Good agreement within numerical integration errors has been found, which serves as a validation of the numerical MB method.

The result for R_b presented here is new. The fermionic electroweak two-loop corrections are found to be relatively large, of the same order as the experimental error of 6.6×10^{-4} . Thus it is important to include these corrections in global electroweak precision fits. For easy use by other groups, a simple parametrization formula has been provided, which accurately approximates the full result within integration errors.

Acknowledgements

This work has been supported in part by the National Science Foundation under grant no. PHY-0854782.

References

- [1] A. Freitas, W. Hollik, W. Walter and G. Weiglein, Phys. Lett. B **495**, 338 (2000) [Erratum-ibid. B **570**, 260 (2003)],
M. Awramik and M. Czakon, Phys. Rev. Lett. **89**, 241801 (2002);
A. Onishchenko and O. Veretin, Phys. Lett. B **551**, 111 (2003);
M. Awramik, M. Czakon, A. Onishchenko and O. Veretin, Phys. Rev. D **68**, 053004 (2003);
M. Awramik and M. Czakon, Phys. Lett. B **568**, 48 (2003).
- [2] A. Freitas, W. Hollik, W. Walter and G. Weiglein, Nucl. Phys. B **632**, 189 (2002) [Erratum-ibid. B **666**, 305 (2003)].
- [3] M. Awramik, M. Czakon, A. Freitas and G. Weiglein, Phys. Rev. D **69**, 053006 (2004).
- [4] M. Awramik, M. Czakon, A. Freitas, G. Weiglein, Phys. Rev. Lett. **93**, 201805 (2004);
M. Awramik, M. Czakon and A. Freitas, Phys. Lett. B **642**, 563 (2006).
- [5] M. Awramik, M. Czakon and A. Freitas, JHEP **0611**, 048 (2006).
- [6] W. Hollik, U. Meier and S. Uccirati, Nucl. Phys. B **731**, 213 (2005);
W. Hollik, U. Meier and S. Uccirati, Nucl. Phys. B **765**, 154 (2007).
- [7] M. Awramik, M. Czakon, A. Freitas and B. A. Kniehl, Nucl. Phys. B **813**, 174 (2009).

- [8] J. J. van der Bij, K. G. Chetyrkin, M. Faisst, G. Jikia and T. Seidensticker, Phys. Lett. B **498**, 156 (2001);
M. Faisst, J. H. Kühn, T. Seidensticker and O. Veretin, Nucl. Phys. B **665**, 649 (2003).
- [9] R. Boughezal, J. B. Tausk and J. J. van der Bij, Nucl. Phys. B **713**, 278 (2005);
R. Boughezal, J. B. Tausk and J. J. van der Bij, Nucl. Phys. B **725**, 3 (2005).
- [10] L. Avdeev, J. Fleischer, S. Mikhailov and O. Tarasov, Phys. Lett. B **336**, 560 (1994) [Erratum-ibid. B **349**, 597 (1994)];
K. G. Chetyrkin, J. H. Kühn and M. Steinhauser, Phys. Lett. B **351**, 331 (1995);
K. G. Chetyrkin, J. H. Kühn and M. Steinhauser, Phys. Rev. Lett. **75**, 3394 (1995).
- [11] K. G. Chetyrkin, J. H. Kühn and M. Steinhauser, Nucl. Phys. B **482**, 213 (1996).
- [12] Y. Schröder and M. Steinhauser, Phys. Lett. B **622**, 124 (2005);
K. G. Chetyrkin, M. Faisst, J. H. Kühn, P. Maierhoefer and C. Sturm, Phys. Rev. Lett. **97**, 102003 (2006);
R. Boughezal and M. Czakon, Nucl. Phys. B **755**, 221 (2006).
- [13] A. B. Arbuzov *et al.*, Comput. Phys. Commun. **174**, 728 (2006).
- [14] H. Flücher, M. Goebel, J. Haller, A. Höcker, K. Mönig and J. Stelzer, Eur. Phys. J. C **60**, 543 (2009) [Erratum-ibid. C **71**, 1718 (2011)].
- [15] C. Anastasiou and A. Daleo, JHEP **0610**, 031 (2006).
- [16] M. Czakon, Comput. Phys. Commun. **175**, 559 (2006).
- [17] J. Gluza, K. Kajda, T. Riemann and V. Yundin, Eur. Phys. J. C **71**, 1516 (2011).
- [18] A. Freitas and Y. C. Huang, JHEP **1004**, 074 (2010).
- [19] G. Degrossi and P. Gambino, Nucl. Phys. B **567**, 3 (2000).
- [20] R. Barbieri, M. Beccaria, P. Ciafaloni, G. Curci and A. Vicere, Phys. Lett. B **288**, 95 (1992) [Erratum-ibid. B **312**, 511 (1993)];
R. Barbieri, M. Beccaria, P. Ciafaloni, G. Curci and A. Vicere, Nucl. Phys. B **409**, 105 (1993);
J. Fleischer, O. V. Tarasov and F. Jegerlehner, Phys. Lett. B **319**, 249 (1993);
J. Fleischer, O. V. Tarasov and F. Jegerlehner, Phys. Rev. D **51**, 3820 (1995).
- [21] K. G. Chetyrkin and F. V. Tkachov, Nucl. Phys. B **192**, 159 (1981);
T. Gehrmann and E. Remiddi, Nucl. Phys. B **580**, 485 (2000).
- [22] S. Bauberger, F. A. Berends, M. Böhm and M. Buza, Nucl. Phys. B **434**, 383 (1995);
S. Bauberger and M. Böhm, Nucl. Phys. B **445**, 25 (1995).

- [23] K. G. Chetyrkin, A. L. Kataev and F. V. Tkachov, Phys. Lett. B **85**, 277 (1979);
M. Dine and J. R. Sapirstein, Phys. Rev. Lett. **43**, 668 (1979);
W. Celmaster and R. J. Gonsalves, Phys. Rev. Lett. **44**, 560 (1980);
S. G. Gorishnii, A. L. Kataev and S. A. Larin, Phys. Lett. B **212**, 238 (1988);
K. G. Chetyrkin and J. H. Kühn, Phys. Lett. B **248**, 359 (1990);
S. G. Gorishnii, A. L. Kataev and S. A. Larin, Phys. Lett. B **259**, 144 (1991);
L. R. Surguladze and M. A. Samuel, Phys. Rev. Lett. **66**, 560 (1991) [Erratum-ibid. **66**, 2416 (1991)];
A. L. Kataev, Phys. Lett. B **287**, 209 (1992);
K. G. Chetyrkin, Phys. Lett. B **307**, 169 (1993).
- [24] K. G. Chetyrkin, J. Kühn and A. Kwiatkowski, in *Reports of the Working Group on Precision Calculations for the Z Resonance*, eds. D. Bardin, W. Hollik and G. Passarino, report CERN 95-03 (1995), pp. 175–263.
- [25] D. Y. Bardin *et al.*, Comput. Phys. Commun. **133**, 229 (2001), sect. 3.6.
- [26] K. Nakamura *et al.* [Particle Data Group], J. Phys. G **37**, 075021 (2010).
- [27] The Tevatron Electroweak Working Group and the CDF and DØ Collaborations, arXiv:1107.5255 [hep-ex];
H. Burkhardt and B. Pietrzyk, Phys. Rev. D **84**, 037502 (2011).
- [28] D. Yu. Bardin, A. Leike, T. Riemann and M. Sachwitz, Phys. Lett. B **206** (1988) 546.
- [29] A. Djouadi and C. Verzegnassi, Phys. Lett. B **195**, 265 (1987);
A. Djouadi, Nuovo Cim. A **100**, 357 (1988);
B. A. Kniehl, Nucl. Phys. B **347**, 86 (1990);
B. A. Kniehl and A. Sirlin, Nucl. Phys. B **371**, 141 (1992);
A. Djouadi and P. Gambino, Phys. Rev. D **49**, 3499 (1994) [Erratum-ibid. D **53**, 4111 (1996)].